Trawl-door Shape Optimization with 3D CFD Models and Local Surrogates

Elvar Hermannsson[1], Leifur Leifsson[2], Slawomir Koziel[2], Piotr Kurgan[2] and Adrian Bekasiewicz[3]
[1]*KTH Royal Institute of Technology, School of Engineering Sciences, Stockholm, Sweden*
[2]*Engineering Optimization & Modeling Center, Reykjavik University, Menntavegur 1, Reykjavik, Iceland*
[3]*Faculty of Electronics, Telecommunications and Informatics, Gdansk University of Technology, 80-233 Gdansk, Poland*

Keywords: Trawl-Door, Ship Fuel Efficiency, Hydrodynamics, Shape Optimization, 3D CFD.

Abstract: Design and optimization of trawl-doors are key factors in minimizing the fuel consumption of fishing vessels. This paper discusses optimization of the trawl-door shapes using high-fidelity 3D computational fluid dynamic (CFD) models. The accurate 3D CFD models are computationally expensive and, therefore, the direct use of traditional optimization algorithms, which often require a large number of evaluations, may be prohibitive. The design approach presented here is a variation of sequential approximate optimization exploiting low-order local response surface models of the expensive 3D CFD simulations. The algorithm is applied to the design of modern and airfoil-shaped trawl-doors.

1 INTRODUCTION

Trawling gear contributes to a majority of the fuel expenditure of many fishing vessels. Fishing gear main parts are the net, a pair of trawl-doors, and a cable extending from the trawl-doors to the boat and the net (see Fig. 1(a)). The role of the trawl-doors is to keep the net open during the trawling operation. Typically, their span is 6-8 m and chord 2-3 m, while the cables are over a few hundred meters long and the net tens of meters. Figure 1(b) shows a modern trawl-door. The trawl-doors may be responsible for roughly 10-30% of the total drag of the entire assembly (Garner, 1967). Good trawl-door designs are therefore desired to minimize fuel consumption.

In general, trawl-doors have remained the same for many decades. This is mainly due to the fact that their designs are based on time-consuming and expensive physical experiments in tow- or flume tanks. Computational fluid dynamics (CFD) is widely used for the design of a variety of vehicles. However, very few CFD-based studies are reported for trawl-doors in the literature (Haraldsson, 1996).

Recently, a design optimization approach for trawl-doors using 2D CFD models has been introduced (Leifsson *et al*., 2014). The approach can be categorized as surrogate-based. As a surrogate model (i.e., a cheaper representation of expensive CFD simulations) it exploits low-order local response surface approximations of the sparsely sampled 2D CFD simulation data.

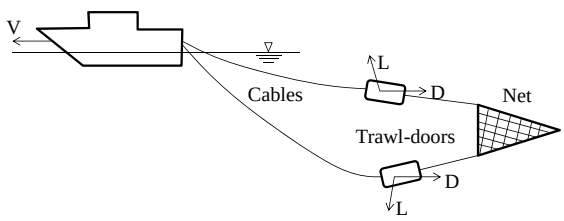

(a)

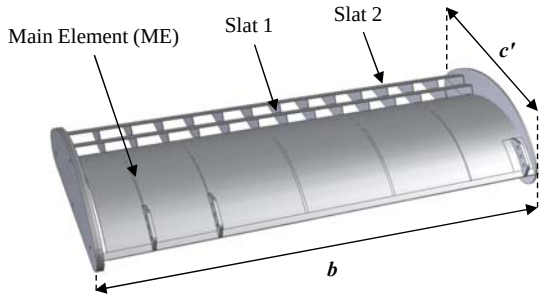

(b)

Figure 1: Schematic of a fishing vessel with trawling gear illustrating (a) the main parts of the fishing gear (not drawn to scale), and (b) a typical trawl-door with two slats.

Hermannsson E., Leifsson L., Koziel S., Kurgan P. and Bekasiewicz A..
Trawl-door Shape Optimization with 3D CFD Models and Local Surrogates.
DOI: 10.5220/0005131307750784
In *Proceedings of the 4th International Conference on Simulation and Modeling Methodologies, Technologies and Applications* (SDDOM-2014), pages 775-784
ISBN: 978-989-758-038-3

2D CFD models are a simplified representation of the flow past trawl-doors. To perform a more realistic and practical design of trawl-doors, 3D CFD models are required to capture the flow physics more accurately. In particular, the trawl-doors are low aspect ratio, and, therefore, the tip vortex will have significant effect on the overall performance. In this paper, we extend our methodology to use 3D CFD models, using the optimized 2D design as a starting point. Although computationally more expensive, the use of 3D CFD simulations turns out to be critical for design reliability.

2 PROBLEM FORMULATION

The design goal is to optimize the shape and configuration of trawl-doors. The design of other components of the trawling gear is not considered here. We setup the trawl-doors using a typical modern shape (Fig. 2(a)) and with airfoil profiles (Fig. 2(b)) as proposed in our earlier work (Jonsson *et al*., 2012; Jonsson *et al*., 2013).

The objective is to minimize the drag of the 3D trawl-door while maintaining a given lift to ensure sufficient opening of the net. In particular, the optimization problem is formulated as

$$\min C_D \tag{1}$$

subject to

$$C_L \geq C_L^* \tag{2}$$

where C_D the drag coefficient (a nondimensional form of the trawl-door drag), C_D is the lift coefficient, and C_L^* is the minimum allowable lift coefficient.

The position and inclination of the elements are the design parameters. The design variable vector can be written as

$$\boldsymbol{x} = [x/c \quad y/c \quad \theta \quad \alpha]^T \tag{3}$$

where x/c is the slat leading-edge position on the x-axis, y/c is the slat leading-edge position on the y-axis, θ is the slat inclination relative to the x-axis, α is the flow angle of attack relative to the x-axis, and c is the length of the main element (c = 1 in this study). Upper and lower bounds, $\boldsymbol{u}$ and $\boldsymbol{l}$, respectively, are prescribed on the design variables.

The size and shape of the elements is fixed. The operating condition, the flow speed V_∞, is also fixed during the optimization.

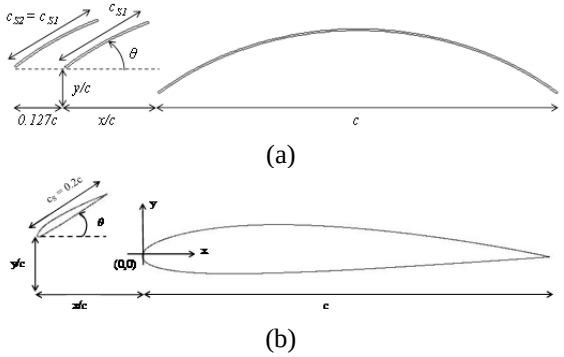

Figure 2: Section cuts of the two shapes, (a) a typical modern trawl-door with thin elements (the F11), and (b) a novel trawl-door with airfoil shaped elements.

3 CFD MODELS

This section describes the CFD models used in this study. In particular, we describe the 2D and the 3D CFD model setup and configuration, as well as give the results of mesh convergence studies and model validation.

3.1 Governing Equations

The flow is assumed steady, incompressible, and viscous. The Reynolds-averaged Navier-Stoke (RANS) equations are taken to be the governing equations with Menter's k-ω SST turbulence model (see, e.g., Tannehill *et al*., 1997).

3.2 Computational Grid

The farfield is configured in a box-topology where the trawl-door geometry is placed in the center of the box. The main element leading edge (LE) is placed as the origin, with the farfield extending 100 chord lengths away from the origin in every direction. Figure 3 shows the 2D solution domain and Fig. 4 shows the 3D one.

The grid is an unstructured triangular one where the elements are clustered around the trawl-door geometry, growing in size as they move away from the origin. The maximum element size on the geometry is set to 0.1% of the chord length. The maximum element size in domain away from the trawl-door is 10 times the chord length. In order to capture the viscous boundary layer well, a prismatic inflation layer is extruded from all surfaces. The initial layer height is chosen so that $y^+ < 1$. The mesh is generated with ICEM CFD (ICEM CFD, 2012). Example meshes is shown in Figs. 5 and 6.

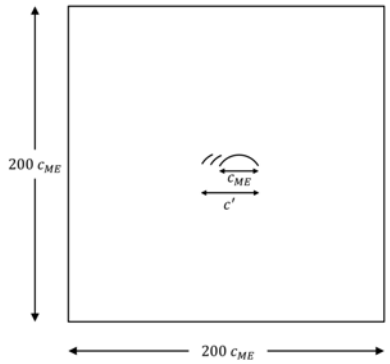

Figure 3: 2D CFD model solution domain.

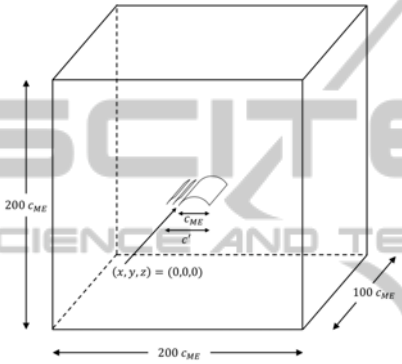

Figure 4: 3D CFD model solution domain.

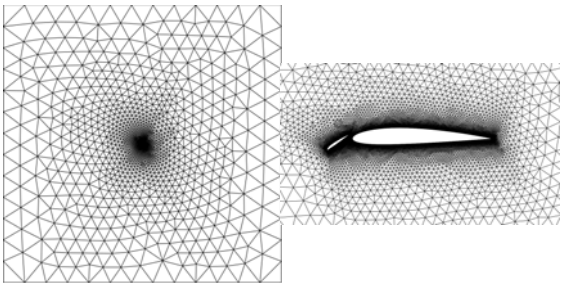

(a) (b)

Figure 5: An example 2D computational grid, (a) the farfield, and (b) a close-up of the trawl-door surface.

3.3 Flow Solver

Numerical fluid flow simulations are performed using the commercial computer code FLUENT (FLUENT, 2012). The flow solver is coupled velocity-pressure-based formulation. A velocity inlet boundary condition is prescribed to all the edges of the farfield, aside from the outlet edge which has a pressure outlet boundary condition.

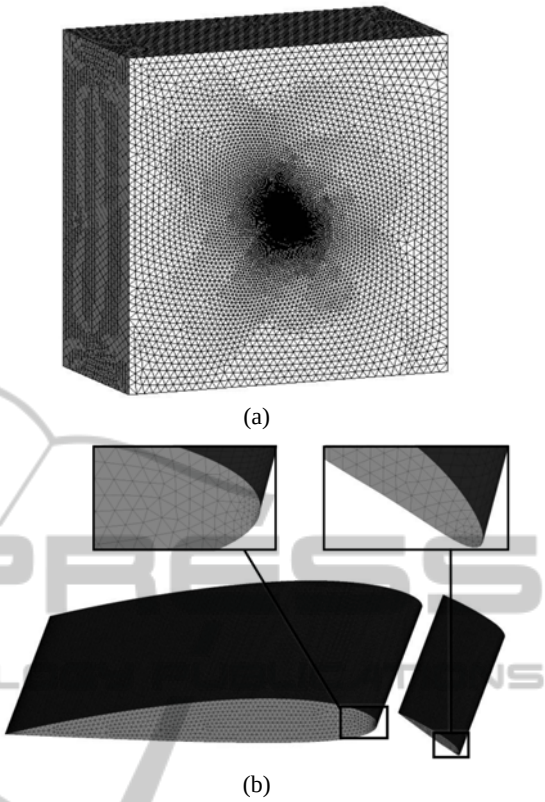

(a) (b)

Figure 6: An example 3D computational grid, (a) the farfield, and (b) a close-up of the trawl-door surface.

The spatial discretization schemes are second order for all flow variables and the gradient information is found using the Green-Gauss node based method. Additionally, due to the difficult flow condition at high angle of attacks, the pseudo-transient option and high-order relaxation terms are used in order to get a stable converged solution. The residuals, which are the sum of the L^2 norms of all governing equations in each cell, are monitored and checked for convergence. The convergence criterion is such that a solution is considered to be converged if the residuals have dropped by six orders of magnitude, or the total number of iterations has reached 6,000 for the 2D model and 2,000 for the 3D model.

3.4 Grid Convergence

A convergence study is performed in order to obtain a grid that is sufficiently fine to capture the flow physics accurately. The methodology of the study is to run the CFD model at the same flow conditions, but with computational grids of various densities. The CFD model should capture the flow characteristics with more accuracy when the grid is

finer. The purpose of the grid convergence study is then to determine the grid density that results in stable simulation results (i.e., not changing upon further grid refinement). The grid satisfying this condition is considered to be converged with respect to the discretization density.

The study is conducted for both 2D and 3D CFD models using a two-element trawl-door configuration with the main element shape of NACA 2410 and a leading-edge slat shape of NACA 3210 (shown in Figs. 5 and 6). The leading-edge of the slat is at $(x/c,y/c) = (-0.20,-0.08)$. The slat is inclined by $\theta_s = 35°$. The free-stream velocity is set at $V_\infty = 2$ m/s, the angle of attack at $\alpha = 20°$ and the Reynolds number is $Re = 2 \cdot 10^6$.

The results of the 2D convergence study shown in Fig. 7(a) indicate that the grid is converged at 168,592 elements, which is the eighth data point, counting from the left - the lower boundary of the *x*-axis. This grid will be used for the 2D CFD model. The simulations were executed using four parallel program nodes, on two Intel Xeon(R) X5660 2.8 GHz processors connected in parallel. The resulting simulation time needed for each of the data points are presented in Fig. 7(b). Inspection of Fig. 7(b) reveals that the simulation runtime decreases significantly from the third to the fourth data point, although the element number is higher. As mentioned before, the convergence criterion is configured in such way that either all of the residuals need to be reduced by six orders of magnitude or that the number of iterations reach up to 6,000. The solution was converged where all residuals had been reduced by six orders after less than 2,500 iterations at the fourth and fifth data points, and that explains the decreased runtime.

The results of the 3D convergence study shown in Fig. 8(a) indicate that the grid is converged at 3,972,136 elements, which is the fifth data point, counting from the left - the lower boundary of the *x*-axis. The number of iterations for each of the simulation runs was 2,000, executed on two Intel Xeon(R) X5660 processors connected in parallel. The resulting time needed for each simulation using the various grids is presented in Fig. 8(b). The simulation time for the chosen 4 million element computational grid is therefore around 26 hours. The simulation time for the sixth data point resulted to be less than for the fifth one, although the number of elements is significantly greater. This is caused by the fact that the solution converged with all residuals reduced by six orders, before the maximum number of iterations was reached.

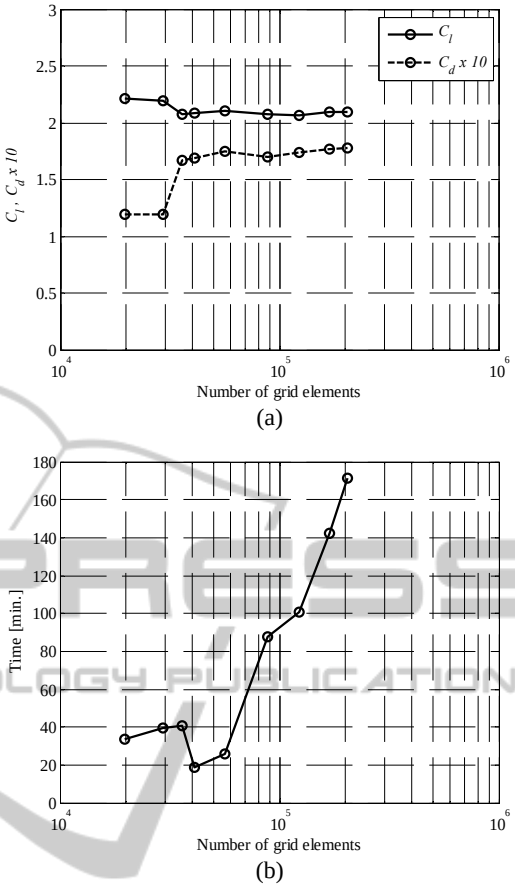

Figure 7: Results of a grid convergence study of the 2D CFD model at $V_\infty = 2$ m/s and $\alpha = 20°$; coefficients of (a) lift and (b) drag versus the number of grid elements.

3.5 Validation

Experimental data is not available for the trawl-door geometries that are used in this study. Consequently, other geometries have to be used to validate the CFD models. For the 2D CFD model, the NACA 0012 airfoil is chosen for the validation process using the data from Ladson (1988). The 3D CFD model is compared against the data by Whicker and Fehlner (1958).

Results for the lift and drag coefficients from the 2D CFD model, compared with the tripped data from Ladson (1988) are presented in Fig. 9. The agreement between computational and experimental data for the lift coefficient versus the angle of attack is excellent up to the stall region where the maximum lift occurs (Fig. 9(a)). However, stall seems to occur at an angle (stall angle of attack) of 16° according to the CFD model, but at an angle of

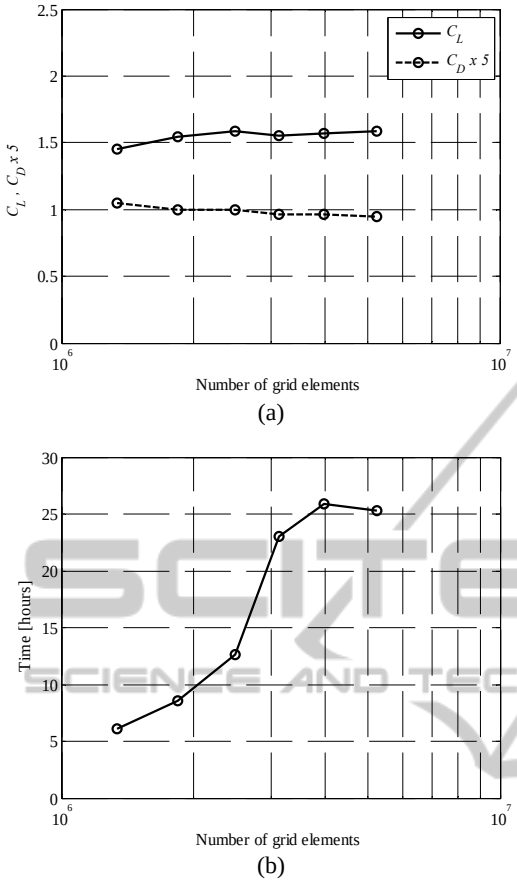

Figure 8: Results of a grid convergence study of the 3D CFD model at V_∞ = 2 m/s and α = 20°; coefficients of (a) lift and (b) drag versus the number of grid elements.

17° according to the experimental data. A graph of the lift coefficient versus the drag coefficient is then presented in Fig. 9(b). Inspection reveals similar results as the preceding graph, the agreement is good up to a point when the flow separation increases. In this case, the agreement is excellent up to a value of the lift coefficient up to around 1.2.

Results for the lift and drag coefficients from the 3D CFD model, compared with the experimental data from Whicker and Fehlner (1958) are presented in Fig. 10. The agreement between the computational and experimental data for the lift coefficient versus the angle of attack is excellent up to a value of around 23° (Fig. 10(a)). According to the experimental data the stall region occurs at around 29°. The computational model is not very reliable when the angle of attack is greater than the stall angle of attack. Very turbulent flow occurs at the stall region, and it should be noted that turbulence modeling is not considered a straight forward task, especially in 3D modeling (Rumsey *et al*., 2010). However, since lift decreases and drag increases when entered into the stall region, it is not feasible to operate under such conditions unless a decrease in velocity is desired. In this study, the aim is to optimize the aerodynamic characteristics of trawl-doors, and therefore the desired operating conditions are at angles less than the stall angle of attack where the validity of the computational model is acceptable. It is however evident that the stall angle of attack is a few degrees smaller according to the computational results, compared to the experimental data. Figure 10(b) shows a comparison between the computational and experimental data of the drag coefficient versus the lift coefficient. This graph indicates a similar behaviour as the preceding ones, stall occurs little earlier in the curve for the computational results, compared with curve for the experimental data. The maximum lift coefficient is therefore lower according to the computational results is around 1.0, whereas it is around 1.3 according to the experimental data.

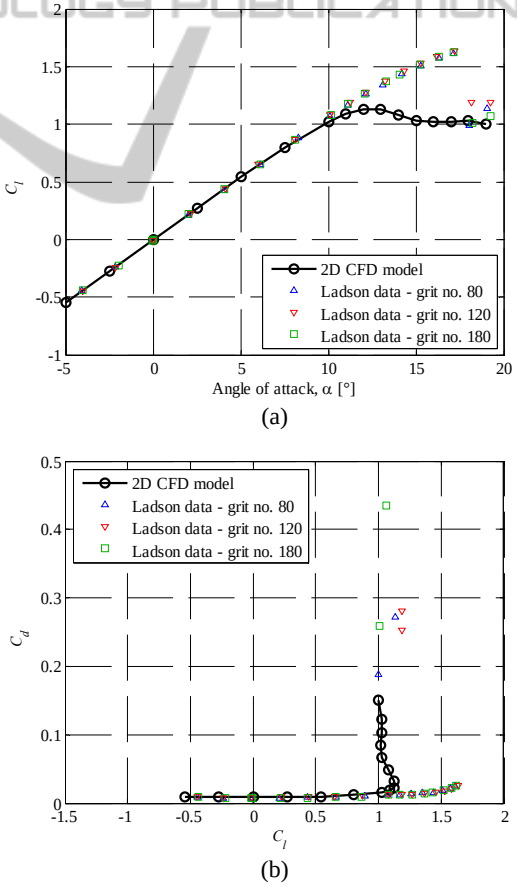

Figure 9: 2D CFD model validation using NACA 0012. Experimental data from Ladson (1988) is shown with triangles and squares.

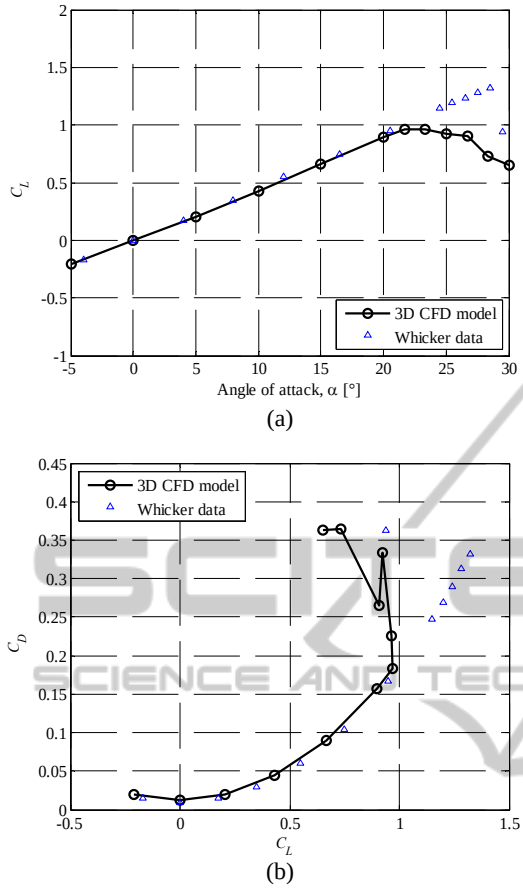

Figure 10: 3D CFD model validation using NACA 0015. Experimental data from Whicker and Fehlner (1958) is shown with the triangles.

4 DESIGN METHODOLOGY

4.1 Formulation

The design problem considered in this work can be formulated as a nonlinear minimization problem of the form

$$\boldsymbol{x}_f^* = \arg\min_{\boldsymbol{x}} U\left(f(\boldsymbol{x})\right) \quad (4)$$

where $f(\boldsymbol{x})$ is the function representing performance parameters of the trawl-door under design (specifically, the lift and the drag coefficients), whereas $\boldsymbol{x}$ is the vector of adjustable geometry parameters; U is a given objective function.

4.2 Optimization by Local Surrogates

The methodology used for trawl-door optimization exploits local response surface approximation (RSA) models. The procedure is iterative. In each iteration, a local model is constructed using sparse samples of f data and low-order polynomial approximation.

Let $\boldsymbol{x}^{(j)} = [x_1^{(j)}\ x_2^{(j)}\ \ldots\ x_n^{(j)}]^T$ be a design obtained as a result of iteration j–1 of the algorithm. Let $\boldsymbol{d}^{(j)} = [d_1^{(j)}\ d_2^{(j)}\ \ldots\ d_n^{(j)}]^T$ be the size parameter that is used to define the vicinity of the vector $\boldsymbol{x}^{(j)}$. The local RSA model is created in the interval $[\boldsymbol{x}^{(j.i)} - \boldsymbol{d}^{(j)}, \boldsymbol{x}^{(j.i)} + \boldsymbol{d}^{(j)}]$. We denote by $X_T^{(j)} = \{\boldsymbol{x}_t^{(j.1)}, \ldots, \boldsymbol{x}_t^{(j.N)}\}$ the training set obtained by sampling the aforementioned vicinity. The response surface approximation (RSA) model is obtained by approximating the data pairs $\{\boldsymbol{x}_t^{(j.k)}, f(\boldsymbol{x}_t^{(j.k)})\}$, $k = 1, \ldots, N$. In this work, a second-order polynomial model $q^{(j)}$ is utilized as follows

$$q^{(j)}(\boldsymbol{x}) = \lambda_0^{(j)} + \sum_{k=1}^{n} \lambda_k^{(j)} x_k + \sum_{k=n+1}^{2n} \lambda_k^{(j)} x_{k-n}^2 \quad (5)$$

The unknown coefficients $\boldsymbol{\lambda} = [\lambda_0\ \lambda_1\ \ldots\ \lambda_n\ \lambda_{11}\ \lambda_{12}\ \ldots\ \lambda_{1n}\ \lambda_{22}\ \ldots\ \lambda_{nn}]$ are found by solving the following the linear regression problems $q(\boldsymbol{x}_t^{(j.k)}) = f(\boldsymbol{x}_t^{(j.k)})\}$, $k = 1, \ldots, N$. The unique solution to this problem exists and can be found analytically assuming that the number of training points is equal or larger than the number of unknown coefficients.

It should be noted that although the used RSA model is very simple, it is sufficient to represent the CFD-simulated model locally. Also, replacing the simulation model by the RSA for the purpose of finding a new candidate design (or, approximated optimum) allows us to alleviate the problem of numerical noise always present in CFD simulations.

4.3 Algorithm Workflow

The optimization algorithm workflow is the following (here, $\boldsymbol{x}^{(0)}$ is the initial design, and $\boldsymbol{d}^{(0)}$ is the initial vicinity size, usually, a fraction of the design space size):

1. Set $j = 0$;
2. Sample the interval $[\boldsymbol{x}^{(j.i)} - \boldsymbol{d}^{(j)}, \boldsymbol{x}^{(j.i)} + \boldsymbol{d}^{(j)}]$ to obtain the training set $X_T^{(j)}$;
3. Evaluate the function f at $X_T^{(j)}$;
4. Identify the RSA model $q^{(j)}$;
5. Find a candidate design, $\boldsymbol{x}^{tmp}$, as
   $\boldsymbol{x}^{tmp} = \arg \min_{\boldsymbol{x}^{(j)} - \boldsymbol{d}^{(j)} \le \boldsymbol{x} \le \boldsymbol{x}^{(j)} + \boldsymbol{d}^{(j)}} U(q^{(j)}(\boldsymbol{x}))$
6. Calculate the gain ratio
   $r = \dfrac{U(f(\boldsymbol{x}^{tmp})) - U(f(\boldsymbol{x}^{(j)}))}{U(q^{(j)}(\boldsymbol{x}^{tmp})) - U(q^{(j)}(\boldsymbol{x}^{(j)}))}$
7. If $r > r_{incr}$, set $\boldsymbol{d}^{(j+1)} = \boldsymbol{d}^{(j)} \cdot m_{incr}$;
8. If $r < r_{decr}$, set $\boldsymbol{d}^{(j+1)} = \boldsymbol{d}^{(j)} / m_{decr}$;
9. If $r > 0$, set $\boldsymbol{x}^{(j+1)} = \boldsymbol{x}^{tmp}$; otherwise $\boldsymbol{x}^{(j+1)} = \boldsymbol{x}^{(j)}$;
10. If the termination condition is satisfied END; else set $j = j + 1$ and go to 2;

In the above procedure, the updating parameters for the trust region size, i.e., r_{incr}, m_{incr}, r_{decr}, and m_{decr} are set by the user. In this work, we set $r_{incr} = 0.75$, $m_{incr} = 1.5$, $r_{decr} = 0.25$, and $m_{decr} = 2$. The algorithm is terminated either if $\| \boldsymbol{x}^{(j+1)} - \boldsymbol{x}^{(j)} \|$ or $\|\boldsymbol{d}^{(j)}\|$ are smaller than a user prescribed threshold. Figure 11 illustrates the operation of the optimization procedure for $n = 2$.

Our optimization algorithm is essentially a trust-region-based procedure with the RSA model used as a prediction tool. The gain ratio r is used to determine the quality of prediction made by the model and, consequently, to update the search radius for the next iteration. In particular, poor prediction power results in reducing the search range (and, at the same time, the validity region for the RSA model). For smaller search range $\boldsymbol{d}$, the RSA model becomes better representation of the CFD-simulated objective. In particular, for sufficiently small $\boldsymbol{d}$, the gain ratio will become positive, i.e., $U(f(\boldsymbol{x}^{tmp})) < U(f(\boldsymbol{x}^{(j)}))$. It should be noted that the expensive CFD is used both to set up the RSA model and to verify the new design. We use a very simple relocation strategy by moving the center of the search region to the new design (upon its acceptance). Upon convergence, the search range is decreased, which, at the same time, leads to improving the accuracy of the RSA model.

5 RESULTS

Design optimization of modern and airfoil-shaped trawl-doors is considered using a 3D CFD model and local surrogates. The design approach is as follows: (1) shape is optimized in 2D, and (2) the optimized design from (1) is used as an initial design for the 3D problem.

5.1 2D Modern Trawl-Door

The objective is to minimize the section drag coefficient (C_d) subject to a constraint on the section lift coefficient ($C_l \geq 1.2$) as described in Section 2. The 2D F11 shape is shown in Fig. 2(a). The design variable vector is $\boldsymbol{x} = [x/c \; y/c \; \theta \; \alpha]^T$ and the search domain is set as: $-0.4 \leq x/c \leq -0.2$, $-0.3 \leq y/c \leq 0.3$, $20° \leq \theta \leq 50°$, $0° \leq \alpha \leq 60°$. The initial design is $x/c = -0.12$, $y/c = -0.0085$, $\theta = 30°$, and $\alpha = -0.19°$. The flow speed is $V_\infty = 2$ m/s and the Reynolds number is $Re = 2 \cdot 10^6$. At this condition, we have $C_l = 1.19$ and $C_d = 0.08$.

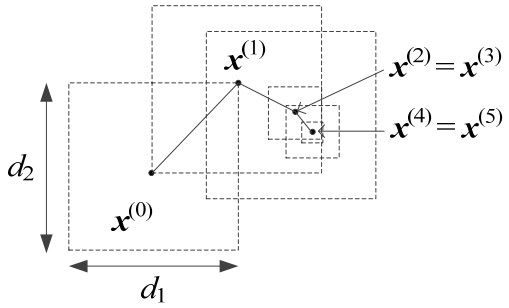

Figure 11: A conceptual illustration of the proposed optimization procedure ($n = 2$).

To solve the optimization problem we use the optimization algorithm described in Section 4. A simple factorial design of experiments (star-distribution) with $2n + 1$ points is used for data sampling. A second order polynomial is used to fit the data, and a gradient-based method (the Matlab (2014) routine *fmincon*) is employed to search for the minima.

The numerical results of the design optimization are presented in Table 1, and the initial and optimum designs are illustrated in Fig. 12. The optimization history with an illustration of the optimization path as well as the vicinity size for each iteration, is presented in Figs. 13 and 14.

The numerical results show that the lift coefficient is held constant while the drag coefficient is reduced by 24%. The resulting increase in the lift-to-drag efficiency is 32% compared with the initial design. The lift coefficient at the optimum design is 1.19, violating the lift constraint by less than 1%. The slat inclination angle hits the lower bound of 20°.

Table 1: Numerical results of the design optimization for the 2D F11 trawl-door.

Variables	Initial	Optimized	Δ
x/c	–0.1200	–0.0544	
y/c	–0.0085	–0.0932	
θ [°]	30.00	20.00	
α [°]	–0.19	2.69	
C_l	1.19	1.19	0%
C_d	0.08	0.06	–24%
C_l/C_d	14.45	19.08	+32%

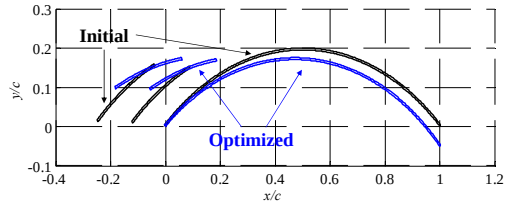

Figure 12: Initial and optimized shapes of the 2D F11 trawl-door. The flow direction is parallel to the *x*-axis.

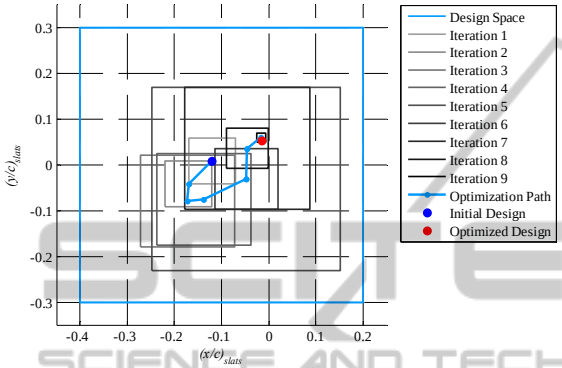

Figure 13: Optimization history of the 2D F11 trawl-door showing the lateral (*x*/*c*) and vertical (*y*/*c*) position of the slats leading-edge.

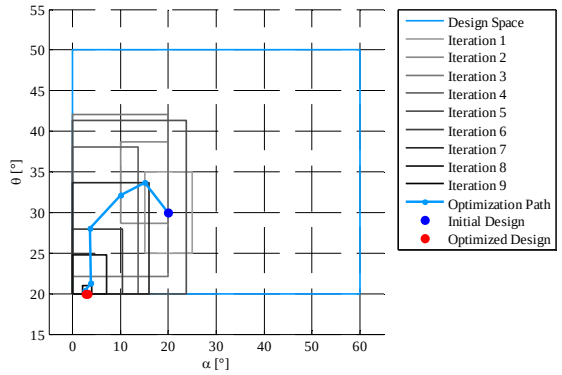

Figure 14: Optimization history of the 2D F11 trawl-door showing the inclination of the slats (θ) and the flow angle of attack (α).

5.2 3D Modern Trawl-Door

The 3D optimization is formulated in the same way as the 2D one described in Section 5.2. However, the minimum lift coefficient is now set as $C_L^* = 1.0$. The initial section shape is set as the optimum design obtained in the 2D case. The span of the trawl-door is set as 6.0 m and the aspect ratio is 2.4.

Table 2: Numerical results of the design optimization for the 3D F11 trawl-door.

Variables	Initial	Optimized	Δ
x/c	–0.0544	–0.0600	
y/c	–0.0932	–0.0732	
θ [°]	20.00	20.00	
α [°]	2.69	0.69	
C_l	1.00	1.00	0%
C_d	0.14	0.13	–6%
C_l/C_d	7.52	7.55	+6%

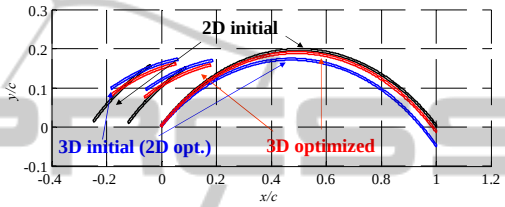

Figure 15: Initial and optimized shapes of the 3D F11 trawl-door. The flow direction is parallel to the *x*-axis.

The numerical results of the 3D design optimization are presented in Table 2. The 3D optimum design, compared with the initial and optimum 2D designs are presented in Fig. 15. The results show that the values for the lift coefficient is held constant while the drag coefficient is reduced by 6% with the corresponding increase by 6% in the lift-to-drag ratio. All the design variables are adjusted slightly, aside from the slat inclination angle, which is still at the lower bound.

5.3 2D Airfoil-Shaped Trawl-Door

The 2D airfoil-shaped trawl-door configuration is shown in Fig. 2(b). The element shapes are kept fixed. The main element has the shape of NACA 2412 and the leading-edge slat has the shape of NACA 3210. The initial design configuration is: x/c = –0.20, y/c = –0.08, θ = 25°, and α = 8.59°. The optimization problem is formulated the same way as described in Section 5.1.

The numerical results of the design optimization are presented in Table 3, and the initial and optimum designs are illustrated in Fig. 16. The optimization history with an illustration of the optimization path as well as the vicinity size for each iteration, is presented in Figs. 17 and 18.

The drag coefficient is reduced by 12% while holding the lift coefficient constant. Again, the slat inclination angle is near the lower bound.

Table 3: Numerical results of the design optimization for the 2D airfoil-shaped trawl-door.

Variables	Initial	Optimized	Δ
x/c	–0.2000	–0.2288	
y/c	–0.0800	–0.0066	
θ [°]	25.00	20.50	
α [°]	8.59	8.28	
C_l	1.20	1.20	0%
C_d	0.020	0.017	–12%
C_l/C_d	60.84	69.88	+12%

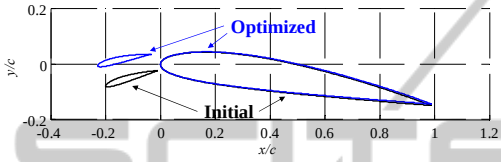

Figure 16: Initial and optimized shapes of the 2D airfoil-shaped trawl-door. The flow direction is parallel to the x-axis.

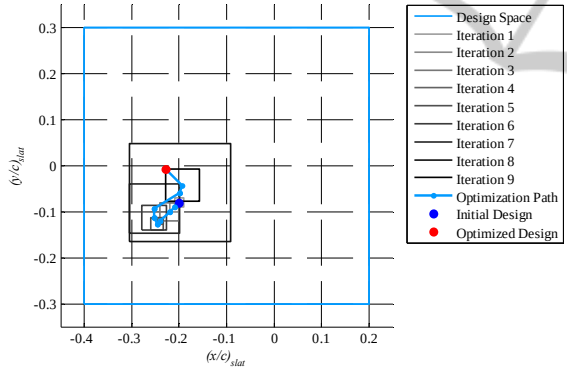

Figure 17: Optimization history of the 2D airfoil-shaped trawl-door showing the lateral (x/c) and vertical (y/c) position of the slats leading-edge.

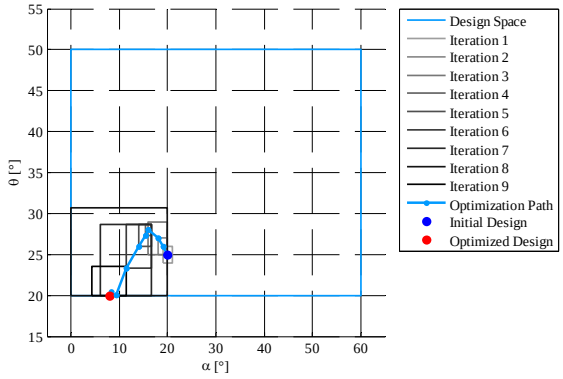

Figure 18: Optimization history of the 2D airfoil-sahped trawl-door showing the inclination of the slats (θ) and the flow angle of attack (α).

5.4 3D Airfoil-Shaped Trawl-Door

The 3D optimization task for the airfoil-shaped trawl-door is formulated in the same way as the 3D optimization of the F11 shape (described in Section 5.2). Table 4 shows the numerical results and Fig. 19 shows the initial and optimized designs.

The drag coefficient is reduced by 5% with the corresponding increase by 6% in the lift-to-drag ratio. There is a significant change is the shape from 2D to 3D indicating the importance of 3D flow effects.

6 CONCLUSION

In this paper, a sequential approximate optimization technique for hydrodynamic design of trawl-door shapes has been presented. The design is based on high-fidelity CFD simulation models. For the sake of design cost reduction as well as reliability of the optimization process, we utilize low-order polynomial models and trust-region framework as a convergence safeguard. Numerical studies are carried out for both 2D and 3D cases with the final designs obtained in a few iterations of the optimization algorithm.

Table 4: Numerical results of the design optimization for the 3D airfoil-shaped trawl-door.

Variables	Initial	Optimized	Δ
x/c	–0.2288	–0.0600	
y/c	–0.0066	–0.0266	
θ [°]	20.50	20.00	
α [°]	7.38	7.21	
C_l	1.00	1.00	0%
C_d	0.050	0.047	–5%
C_l/C_d	14.56	15.76	+6%

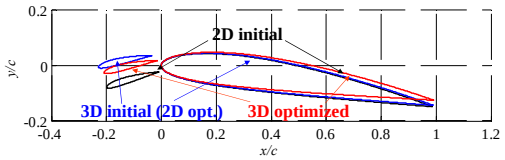

Figure 19: Initial and optimized shapes of the 3D airfoil-shaped trawl-door. The flow direction is parallel to the x-axis.

REFERENCES

FLUENT, ver. 14, ANSYS Inc., Southpointe, 275 Technology Drive, Canonsburg, PA 15317, 2012.

Garner, J., *Botnvarpan og bunadur hennar*, Fiskifelag Islands, 1967.

Haraldsson, H.O., "Fluid Dynamics Simulation of Fishing Gear," M.Sc. Thesis, University of Iceland, May 1996,

ICEM CFD, ver. 14, ANSYS Inc., Southpointe, 275 Technology Drive, Canonsburg, PA 15317, 2012.

Jonsson, E., Leifsson, L., and Koziel, S. "Trawl-Door Performance Analysis and Design Optimization with CFD", 2nd Int. Conf. on Simulation and Modeling Methodologies, Technologies, and Applications (SIMULTECH), Rome, Italy, July 28-31, 2012.

Jonsson, E., Hermannsson, E., Juliusson, M., Koziel, S., and Leifsson, L. "Computational Fluid Dynamic Analysis and Shape Optimization of Trawl-Doors," 51st AIAA Aerospace Sciences Meeting including the New Horizons Forum and Aerospace Exposition, Grapevine, Texas, January 7-10, 2013.

Ladson, C.L., "Effects of Independent Variation of Mach and Reynolds Numbers on the Low-Speed Aerodunamic Characteristics of the NACA 0012 airfoil Section," NASA Technical Memorandum 4074, NASA, 1988.

Leifsson, L., Koziel, S., Hermannsson, E., and Reza Fakhraie, "Trawl-Door Design Optimization by Local Surrogate Models," *55th AIAA/ASMe/ASCE/AHS/SC Structures, Structural Dynamics, and Materials Conference*, National Harbor, MD, January 2014.

Matlab, ver. R2014a, The Mathworks Inc., Natick, Massachusetts, U.S.A, 2014.

Rumsey, C. L., Smith, B. R., and Huang, G. P., "Description of a Website Resource for Turbulence Modeling Verification and Validation," *40th AIAA Fluid Dynamics Conference and Exhibit*, AIAA Paper 2010-4742, Chicago, U.S.A., July 2010.

Tannehill, J.A., Anderson, D.A., and Pletcher, R.H., *Computational fluid mechanics and heat transfer*, 2nd edition, Taylor & Francis, 1997.

Whicker, L. F., and Fehlner, L. F. "Free-Stream Characteristics of a Family of Low-Aspect Ratio, All-Movable Control Surfaces for Application to Ship Design," National Technical Information Service, U.S. Department of Commerce, U.S.A, December 1958.